





## RESEARCH ARTICLE

# Cell-surface contacts determine volume and mechanical properties of human embryonic kidney 293 T cells

Venkata A. S. Dabbiru<sup>1,2,3</sup>  | Emmanuel Manu<sup>1,2,3</sup> | Doreen Biedenweg<sup>1,3</sup>  | Peter Nestler<sup>1,3</sup>  | Ricardo H. Pires<sup>1,2,3</sup> | Oliver Otto<sup>1,2,3</sup> 

<sup>1</sup>Zentrum für Innovationskompetenz: Humorale Immunreaktionen bei kardiovaskulären Erkrankungen, Universität Greifswald, Greifswald, Germany

<sup>2</sup>Deutsches Zentrum für Herz-Kreislauf-Forschung e.V. Standort Greifswald, Universitätsmedizin Greifswald, Greifswald, Germany

<sup>3</sup>Institut für Physik, Universität Greifswald, Greifswald, Germany

## Correspondence

Oliver Otto, Institut für Physik, Universität Greifswald, Felix-Hausdorff-Strasse 6, 17489 Greifswald, Germany.

Email: [oliver.otto@uni-greifswald.de](mailto:oliver.otto@uni-greifswald.de)

## Funding information

German Federal Ministry of Education and Research, Grant/Award Number: 03Z22CN11, 03Z22C511; German Center for Cardiovascular Research, Grant/Award Number: 81X3400107

## Abstract

Alterations in the organization of the cytoskeleton precede the escape of adherent cells from the framework of cell–cell and cell–matrix interactions into suspension. With cytoskeletal dynamics being linked to cell mechanical properties, many studies elucidated this relationship under either native adherent or suspended conditions. In contrast, tethered cells that mimic the transition between both states have not been the focus of recent research. Using human embryonic kidney 293 T cells we investigated all three conditions in the light of alterations in cellular shape, volume, as well as mechanical properties and relate these findings to the level, structure, and intracellular localization of filamentous actin (F-actin). For cells adhered to a substrate, our data shows that seeding density affects cell size but does not alter their elastic properties. Removing surface contacts leads to cell stiffening that is accompanied by changes in cell shape, and a reduction in cellular volume but no alterations in F-actin density. Instead, we observe changes in the organization of F-actin indicated by the appearance of blebs in the semi-adherent state. In summary, our work reveals an interplay between molecular and mechanical alterations when cells detach from a surface that is mainly dominated by cell morphology.

## KEYWORDS

atomic force microscopy, cell mechanics, cell-surface contacts, F-actin, real-time deformability cytometry

## 1 | INTRODUCTION

The mechanical properties of cells reflect both the physiological development of cellular processes as well as signal the emergence of pathological states. Changes in mechanical properties have been noticed in differentiating cells (Maloney et al., 2010; Steward & Kelly, 2015), cell migration (Lautenschläger et al., 2009), throughout the cell cycle (Otto et al., 2015), as well as in cells undergoing oncological processes (Frank Sauer et al., 2021; Lekka & Pabijan, 2019), or responding to inflammatory conditions (Ekpenyong et al., 2015).

These and other studies have established the importance of mechanical properties as a sensitive biomarker of cellular response to a dynamic microenvironment.

The cytoskeleton is a pivotal element in defining the mechanical properties of the cell, is responsible for maintaining the integrity of cell shape, and drives morphological changes in response to internal triggers (Fletcher & Mullins, 2010). But the cytoskeleton is also responsive to external cues, such as the chemical composition and the physical properties, for example, stiffness, or topography of the surface on which cells grow. A combination of these factors ultimately

This is an open access article under the terms of the [Creative Commons Attribution-NonCommercial](https://creativecommons.org/licenses/by-nc/4.0/) License, which permits use, distribution and reproduction in any medium, provided the original work is properly cited and is not used for commercial purposes.

© 2022 The Authors. *Cytoskeleton* published by Wiley Periodicals LLC.

contributes to the definition of the physiological state of cells (Denning et al., 2016). The interplay between cell physiology and physical signals is particularly accentuated for adherent cells which communicate with their microenvironment via a myriad of cell-surface receptors, including attachment complexes. Availability of cryptic sites in such complexes to the extracellular matrix (ECM) is regulated by the conformational changes, thus enabling the adherent cells to transiently or altogether detach from their surface and loose interactions with the ECM (Wolfenson et al., 2009). Cytoskeletal modifications during such transitions indeed facilitate cell migration, for instance, during the onset of metastasis (Fife et al., 2014). These cytoskeletal alterations are often largely governed by the F-actin network, which is a major component of the cytoskeleton that responds to external physical and chemical cues, mediating a variety of cellular events beyond cell adhesion and migration (Stricker et al., 2010). Earlier reports have already indicated that F-actin levels and its organization have also been linked to changes in the mechanical properties of cells. For example, higher levels of F-actin were shown to increase the elasticity of Vero cells grown in a monolayer (Efremov et al., 2013). Another study associated the increased thickness of stress fibers in mesenchymal stem cells with increased cell stiffness (Maloney et al., 2010). Similarly, it has been shown that the F-actin organization as a perinuclear actin cap is essential for defining the elastic properties of mesenchymal stem cells (Kihara et al., 2011).

Over the years a variety of studies have examined and demonstrated the association between the cytoskeletal organization and mechanical properties of cells in suspension or in the context of a surface to which they are adhered to. However, fewer studies have addressed the consequences associated with cell-surface detachment (Buonsanti et al., 2009; Maloney et al., 2010). Given that most methods typically require cells to either be in the suspended or in the adherent state, the challenge is found in efficiently tracking and mechanically probing cells as they transit between both states.

To address this problem, we made use of two distinct methods to assess cell elasticity. We employed atomic force microscopy (AFM) to probe human embryonic kidney 293 T (HEK293T) cells in their adherent and tethered states while using real-time deformability cytometry (RT-DC) to characterize them in suspension. First, we analyzed the dependence of seeding density on the size and elasticity of individual cells. To mimic a transition between the adherent and suspended states, we promoted surface-immobilization of cells via unspecific linker molecules, which passively tethered them to the substrate. These semi-adherent cells were mechanically probed by AFM. To identify possible cytoskeletal and morphological changes associated with the three different states we resorted to fluorescent imaging of the F-actin network. We found that the transition from adherent to suspension state is accompanied by a decrease in cellular volume and correlates with an increase in cell elasticity. Interestingly, these changes are not accompanied by variations in the amount of filamentous actin but seem to be linked to the organization of F-actin and the overall cell morphology.

## 2 | RESULTS

### 2.1 | Seeding density does not affect cell elasticity

We first studied how the seeding density affects the mechanical properties of HEK293T cells grown at  $16 \times 10^3$ ,  $40 \times 10^3$ ,  $100 \times 10^3$ , and  $160 \times 10^3$  cells/cm<sup>2</sup>, respectively (Figure S1). To assess the dependency of the cellular elasticity on the seeding density in a statistically robust manner, we employed RT-DC for which we collected thousands of single-cell measurements per condition (see Methods). Analyzing the deformation vs. cell size over a range between  $16 \times 10^3$  cells/cm<sup>2</sup> (Figure 1a, upper left panel) and  $160 \times 10^3$  cells/cm<sup>2</sup> (Figure 1a, upper right panel) revealed no apparent difference in deformation but a qualitative reduction in size when cells were cultured at high seeding density (Figure S2). Calculating Young's modulus using an analytical and numerical model (see Methods) reveals an elasticity that seems to be independent of the seeding density (Figure 1a, lower panel and Figure S3).

A statistical analysis using linear mixed models (see Methods) on three or more independent experimental replicates per condition summarizing 44,058 cells ( $16 \times 10^3$  cells/cm<sup>2</sup>), 17,381 cells ( $40 \times 10^3$  cells/cm<sup>2</sup>), 16,944 cells ( $100 \times 10^3$  cells/cm<sup>2</sup>) and 9,457 cells ( $160 \times 10^3$  cells/cm<sup>2</sup>) respectively, confirms the observed trend. While cell deformation remains constant (Table S1), we find a consistent and statistically significant decrease in cell size from  $212 \pm 2 \mu\text{m}^2$  (mean  $\pm$  SEM) to  $193 \pm 3 \mu\text{m}^2$  with increasing seeding density (Figure 1b). In contrast, within the experimental error of the measurements, Young's modulus is constant for all conditions analyzed (Figure 1c) confirming that cell elasticity appears to be independent of the seeding density. Subsequently, we chose to continue our work by probing cells at a density of approximately 30,000 cells/cm<sup>2</sup>.

### 2.2 | Detachment induces cell stiffening

Having verified that seeding density does not impact cell elasticity, we next investigated the role of surfaces and surface contacts for cell mechanical properties. We examined HEK293T cells under three conditions. After having grown cells on tissue culture-treated surfaces (see Methods), they were either studied directly on those surfaces (Figure 2a) or proteolytically detached and allowed to re-settle on a surface coated with bio-anchor molecules (BAM, Figure 2b). BAM molecules contain a terminal oleic acid moiety that allows for the non-specific interaction of the BAM layer with the cell membrane. This configuration enables passive cellular immobilization via tethering without any requirement to form surface adhesion complexes. Under adherent and tethered conditions, cells were probed by atomic force microscopy (AFM). In addition, the mechanical properties of HEK293T cells in suspension were also studied by RT-DC immediately following detachment (Figure 2c).

In the current study, AFM indentation measurements were carried out with a colloidal probe attached to a calibrated flexible

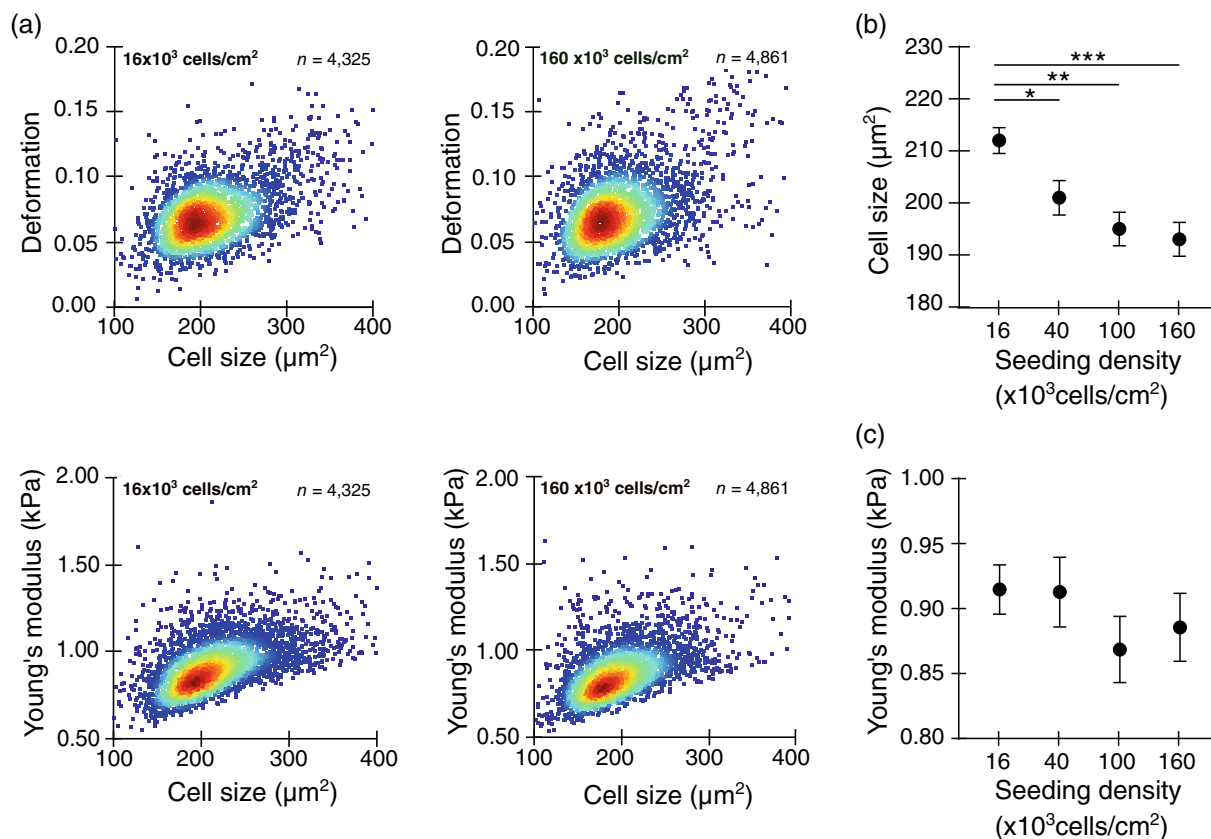
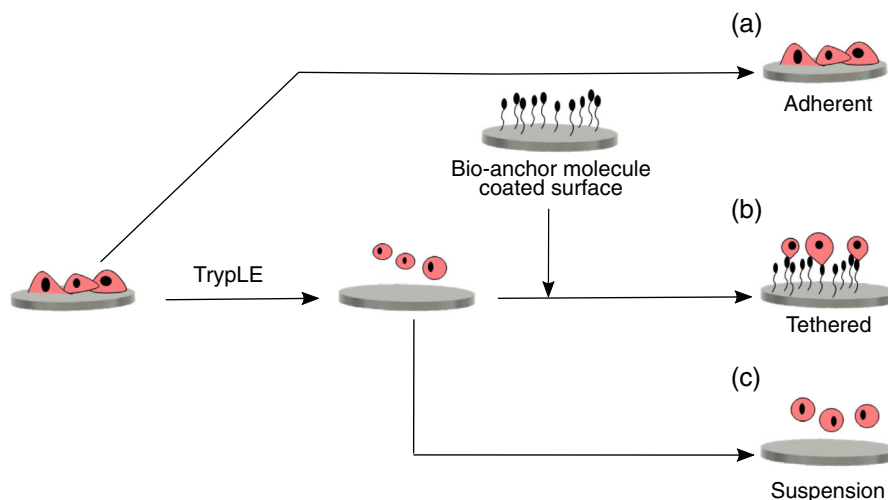


**FIGURE 1** Impact of seeding density on mechanical properties of HEK293T cells in suspension. (a) Scatter plots of deformation vs. cell size (upper panel) and Young's modulus vs. cell size (lower panel) of HEK293T cells at seeding densities of  $16 \times 10^3$  and  $160 \times 10^3$  cells/cm<sup>2</sup>. Statistical analysis of (b) mean cell size and (c) Young's modulus of three experimental replicates at seeding densities of  $16 \times 10^3$ ,  $40 \times 10^3$ ,  $100 \times 10^3$  and  $160 \times 10^3$  cells/cm<sup>2</sup> consisting of 87,840 events in total. RT-DC measurements were carried out in a  $30 \times 30 \mu\text{m}^2$  channel at a flow rate of  $0.24 \mu\text{l/s}$ . Statistical analysis was carried out using linear mixed models. Error bars represent standard error of the mean (\* $p < 0.05$ ; \*\* $p < 0.01$ ; \*\*\* $p < 0.001$ )

**FIGURE 2** Schematics of sample preparation. HEK293T cells were cultured to attain an approximate density of  $30,000$  cells/cm<sup>2</sup> and probed in (a) adherent state or (b) proteolytically detached and tethered to a surface by a non-specific bio-anchor molecule (BAM) or (c) suspension state after detachment



cantilever (Cappella, 2016; Haase & Pelling, 2015). Each individual experiment results in a force-distance curve that follows a parabolic profile upon contact with the cells, and where the steepness of the force gradient informs on Young's modulus. These force gradients can be visualized as isoelasticity lines (blue lines in Figure 3a), along which the increasing force is associated with a specific Young's modulus.

Several such measurements were recorded on different cells, encompassing a minimum of 25 different locations per cell. Evaluating force-distance curves of adherent HEK293T cells (black lines in Figure 3a, top panel) yielded a median Young's modulus  $\bar{E} \approx 200\text{Pa}$  (green line in Figure 3a, top panel). Limiting the capability of cells to actively adhere to a surface and allowing only passive attachment by BAM resulted in

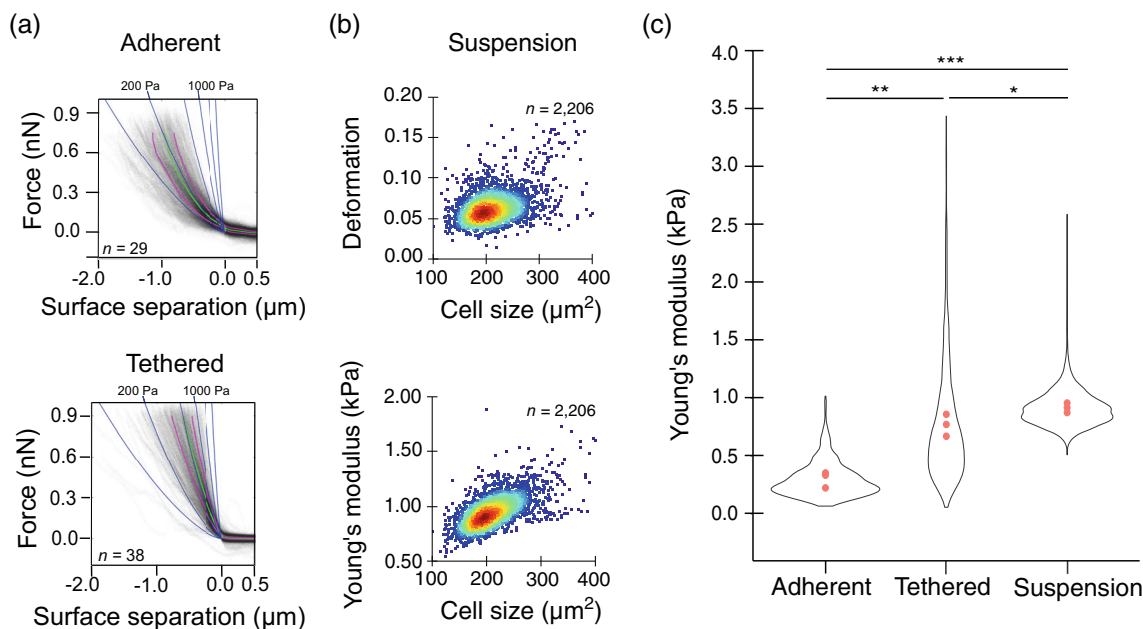


**FIGURE 3** Impact of cell-surface interactions on mechanical properties of HEK293T cells. (a) Force spectroscopy measurements performed on adherent (upper panel) and tethered (lower panel) cells with force-distance curves (black lines), median (green line), and interquartile range (magenta lines). Iso-elasticity lines (blue) are lines of constant Young's modulus. (b) Scatter plot of deformation vs. cell size (upper panel) and Young's modulus vs. cell size (lower panel) for suspended cells. Measurements were carried out in a  $30 \times 30 \mu\text{m}^2$  channel at a flow rate of  $0.24 \mu\text{l/s}$ . (c) Statistical analysis of three independent biological replicates per condition for cells in adherent state ( $n = 29$ ), in tethered state ( $n = 38$ ) and in suspension ( $n = 10,163$ ). Significances were calculated from linear mixed models. Error bars represent standard errors of the mean. Red data points represent mean values of respective replicates (\* $p < 0.05$ ; \*\* $p < 0.01$ ; \*\*\* $p < 0.001$ )

an increase to  $\bar{E} \approx 600\text{Pa}$  (green line in Figure 3a, bottom panel), which suggests that even in the context of passive immobilization, a reduction in the number and formation of focal adhesion sites induces cell stiffening. Finally, removing all surface constraints and analyzing cells in suspension by RT-DC (see Methods), we found a single population with characteristic cell size and deformation values (Figure 3b, top panel) corresponding to an elastic modulus of approximately  $900\text{Pa}$  (Figure 3b, bottom panel).

A statistical analysis of experimental replicates with a total of  $n = 29$  cells encompassing 688 data points (adherent),  $n = 38$  cells with 911 data points (tethered), and  $n = 10,163$  cells (suspension) confirmed the trend, where the loss of surface contacts induces a significant stiffening of the cells (Figure 3c and Figure S4). We determined a mean Young's modulus of  $\bar{E} = 0.27 \pm 0.02\text{kPa}$  for adherent cells,  $\bar{E} = 0.63 \pm 0.06\text{kPa}$  for the tethered state and  $\bar{E} = 0.90 \pm 0.08\text{kPa}$  for cells measured in suspension. The large standard error of the mean in elasticity obtained for cells that were passively attached to a surface suggests a non-homogeneous distribution of cells with contributions from adherent and suspension properties.

### 2.3 | Cell elasticity is directed by cell morphology but not by F-Actin density

Having identified cell elasticity as a mechanical property being dependent on the extent of cell-surface attachment, we attempted to establish possible links to the cytoskeleton. In our experiments, adherent,

tethered, and suspended cells were labeled for F-actin and imaged via confocal laser scanning microscopy at magnifications of  $20\times$  (Figure 4a, upper panel) and  $63\times$  (Figure 4a, lower panel, see Methods). Imaging revealed that adherent HEK293T cells are spread out, while suspended and tethered cells possess a globular shape, with the latter evidencing signs of blebbing (Figure 4a, center and right columns). Formation of blebs was already described as the response of the suspended cells to deal with excess membrane after loss of surface contacts (Maloney et al., 2010), especially during the reattachment efforts of the cells to the surface. In line with previous reports (Guo, Wang, et al., 2014; Haghparast et al., 2015) confocal imaging did not reveal any stress fibers in HEK293T cells (Figure 4a). Therefore, these structures were not considered in our analysis.

Following reports suggesting that alterations in cell mechanical properties occurring during a surface detachment are mediated by the F-actin network (Chan et al., 2015; Maloney et al., 2010), we were interested in understanding if the increase in cell elasticity could be linked to alterations in the density of F-actin in the entire cell or if it would be localized to the cortical region. F-actin density was calculated by integrating the fluorescence intensity of the TRITC-phalloidin signal for a given focal plane (with highest signal strength) and dividing it by the respective cell area. In total, we analyzed  $n = 229$  cells in experimental triplicates under these conditions (see Methods).

We assessed the average F-actin density of the whole cell to be  $1.03 \pm 0.20 \mu\text{m}^{-2}$  for the adherent state,  $1.12 \pm 0.22 \mu\text{m}^{-2}$  for the tethered state, and  $0.84 \pm 0.17 \mu\text{m}^{-2}$  in the suspended state (Figure 4b, left panel). Given that no statistically significant difference

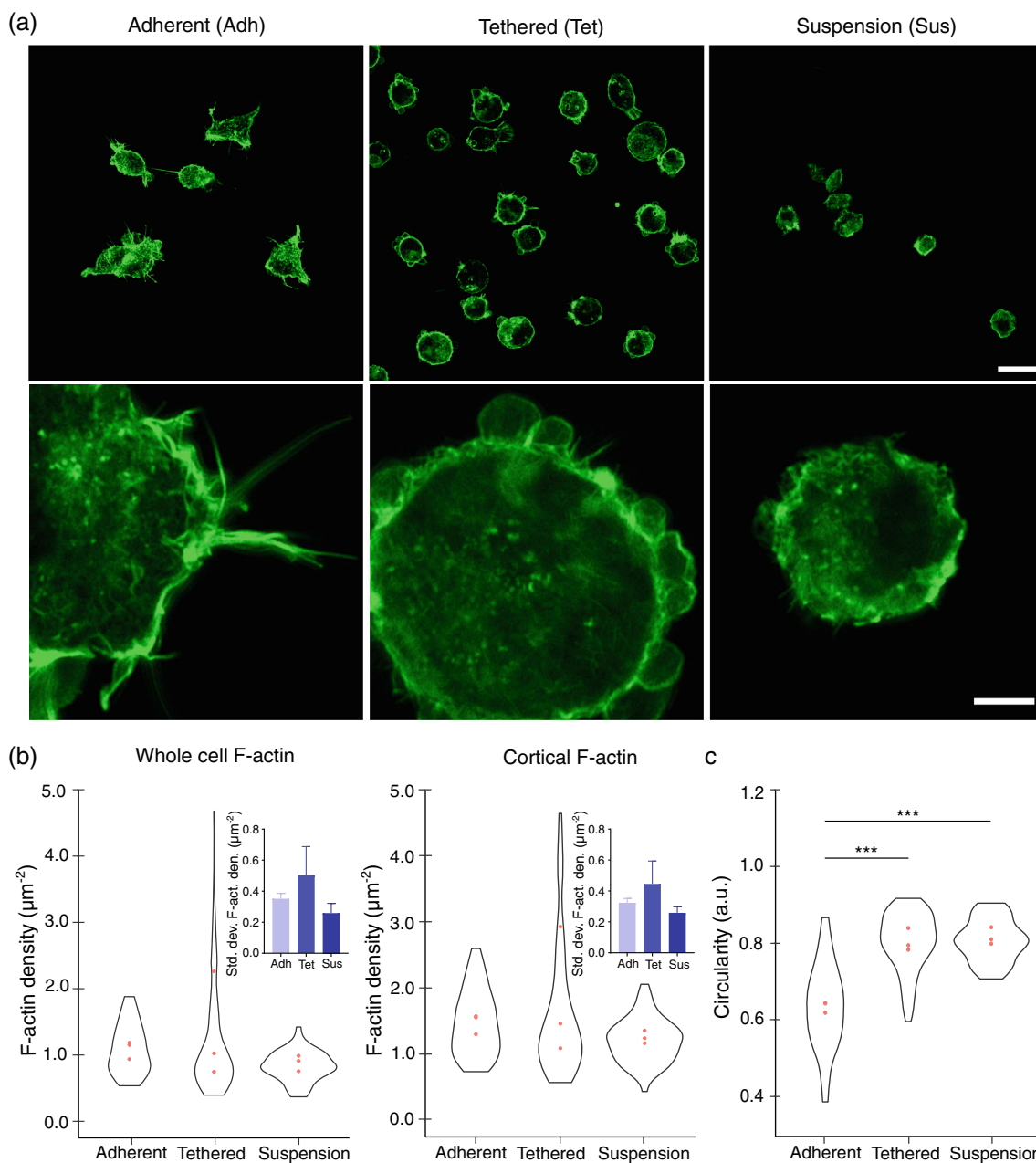


**FIGURE 4** Effect of surface interactions on F-Actin levels and cell morphology. (a) Confocal microscopy images of adherent, tethered and suspended cells labeled for F-Actin. Scale bars are 25  $\mu\text{m}$  (upper panel) and 5  $\mu\text{m}$  (lower panel). (b) Statistical analysis of three experimental replicates for adherent (Adh), tethered (Tet) and suspended (Sus) cells displaying F-Actin levels in the whole cell (left panel) and cortical F-Actin (right panel). Insets show the mean of the standard deviations of individual replicates. (c) Statistical analysis of cell circularity for experimental replicates is shown in (b). Analysis summarizes  $n = 61$  adherent cells,  $n = 113$  tethered cells, and  $n = 55$  suspended cells and has been performed using linear mixed models. Red data points represent mean values of respective replicates. Error bars represent standard errors of the mean (\*\*\*)  $p < 0.001$

was detected between these conditions, we selectively looked at the cortical region, which we defined as a shell of 1  $\mu\text{m}$  width from the cell periphery (see Methods). As with the case of the entire cell, the amount of F-actin localized in the cortical region seems to be unaffected by the presence of a surface and our analysis yields mean intensities of  $1.40 \pm 0.24 \mu\text{m}^{-2}$  when cells are kept adhered to a surface,  $1.56 \pm 0.26 \mu\text{m}^{-2}$  in tethered state and  $1.20 \pm 0.21 \mu\text{m}^{-2}$  in suspension (Figure 4b, right panel). However, our data indicated that

irrespective of the adhesion state, cells typically show a significantly higher density of F-actin in the cortex relative to the rest of the cell body ( $p < 0.0001$ ).

Next, we speculated if the pronounced variation in Young's modulus for tethered cells (Figure 3c) can be understood from alterations in the F-actin density. Determining the standard deviation in filamentous actin density between individual cells, we found a maximum of  $0.51 \pm 0.18 \mu\text{m}^{-2}$  for the tethered state compared to 0.35

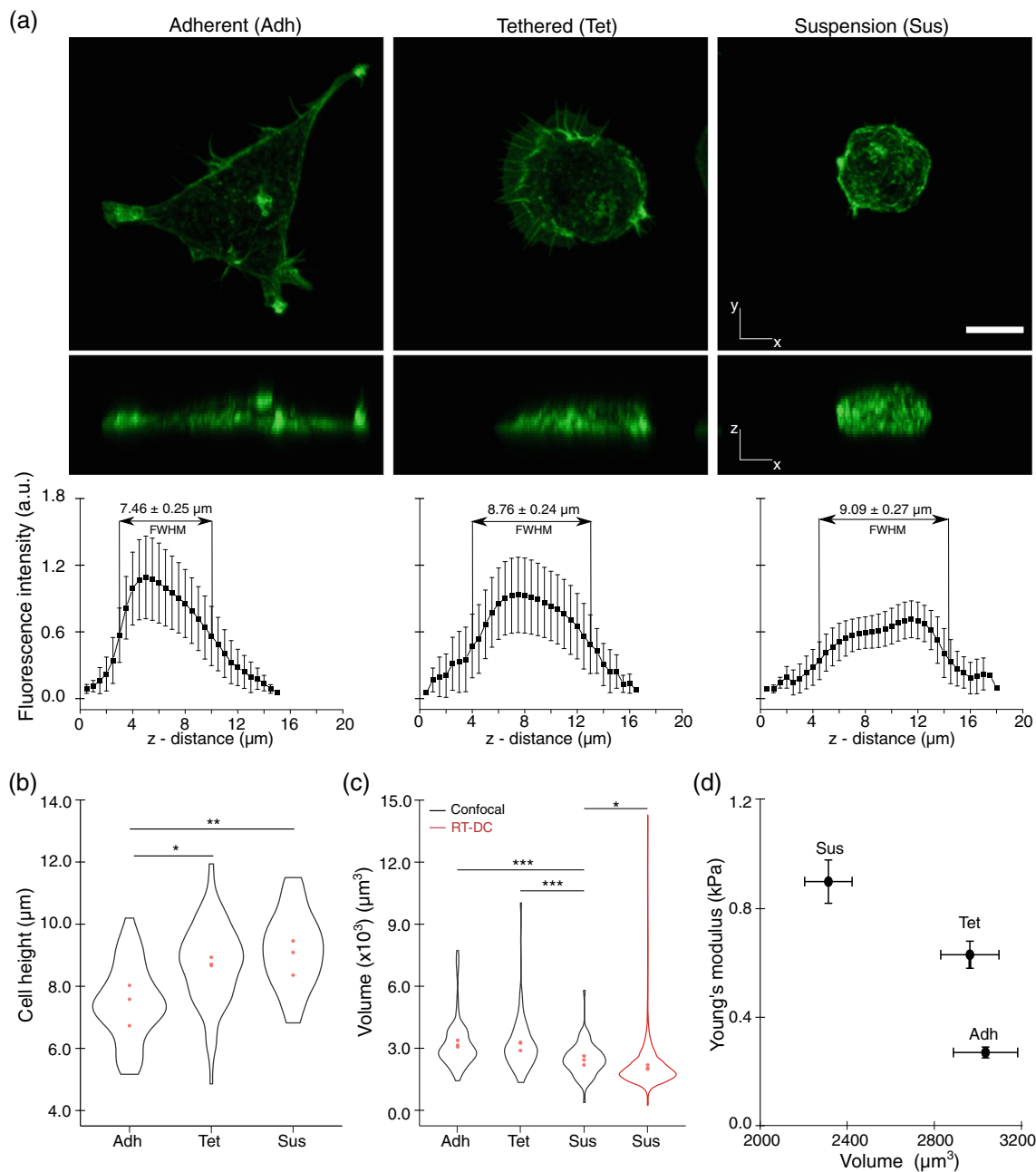


**FIGURE 5** Effect of surface interaction on cell height and volume. (a) Example images of cells in adherent, tethered and suspension states immobilized on a surface and visualized by maximum intensity projections in the  $xy$ -plane (upper panel), and in the  $xz$ -plane (middle panel). Scale bar  $10\ \mu\text{m}$ . Lower panel shows the integrated fluorescence intensity per slice from  $z$ -stack as a measure of cell height (full width at half maximum, FWHM). (b) Statistical analysis of cell height by considering the FWHM of the fluorescence signal along the  $z$ -axis for adherent (Adh,  $n = 60$ ), tethered (Tet,  $n = 70$ ) and suspended (Sus,  $n = 47$ ) cells. (c) Statistical analysis of volume for adherent ( $n = 66$ ), tethered ( $n = 81$ ) and suspended ( $n = 73$ ) cells (confocal microscopy data, black violin plots). Red violin plot summarizes  $n = 6,582$  cells where volume has been calculated from RT-DC reservoir data. (d) Mean Young's modulus vs. cell volume. Young's modulus was deduced by AFM for adherent and tethered cells while RT-DC was employed for suspended cells. Cell volume is taken from (c) displaying data from confocal microscopy images only. Error bars represent standard error of the mean. Statistical analyses were performed on three experimental replicates using linear mixed models. Red data points represent mean values of respective replicates ( $*p < 0.05$ ;  $**p < 0.01$ ;  $***p < 0.001$ )

$\pm 0.03\ \mu\text{m}^{-2}$  and  $0.26 \pm 0.06\ \mu\text{m}^{-2}$  when cells are adhered to a surface or in suspension, respectively (Figure 4b, inset left panel). An analysis of the cortical actin data revealed similar non-significant results of standard deviations of  $0.66 \pm 0.21\ \mu\text{m}^{-2}$  (tethered state),

$0.48 \pm 0.04\ \mu\text{m}^{-2}$  (adherent cells), and  $0.38 \pm 0.05\ \mu\text{m}^{-2}$  (suspension cells, Figure 4b, inset right panel).

Since alterations in F-actin density could not explain the observed variations in cell elasticity, we next examined the circularity of cells,



which, according to earlier reports was found to be an important morphological feature associated with cell mechanical properties (Tachibana et al., 2015). A statistical analysis on almost 200 cells revealed the mean circularity for adherent cells to be  $0.63 \pm 0.01$  and significantly smaller ( $p < 0.001$ ) than cells in tethered ( $0.80 \pm 0.01$ ) and suspended states ( $0.81 \pm 0.01$ , Figure 4c).

## 2.4 | Loss of cell-surface contacts correlates with changes in cellular volume

Alterations in cell mechanical properties with respect to surface attachment appeared to be more correlated with morphological differences than with changes in the levels of F-actin. Therefore, we investigated possible differences in cell height and volume using z-stack images obtained at  $20\times$  magnification of TRITC-phalloidin labeled cells (see Methods). As HEK293T cells detach from a surface, they engage in a considerable increase in cell height (Figure 5a). When being fully adhered to a surface, cells are spread out, while the tethered cells showed cell rounding as reported before (Tachibana et al., 2015), which accentuates to suspension state. We quantify this observation by calculating a representative cell height utilizing the full width at half maximum (FWHM) of the F-actin fluorescence intensity distribution along the z-stack (see Methods, Figure 5b). Analyzing experimental triplicates of a total of  $n = 60$  adherent,  $n = 70$  tethered and  $n = 47$  suspended cells confirmed the above observation. Mean FWHM values showed a significant increase in cell height from  $7.46 \pm 0.25 \mu\text{m}$  for adherent cells, to  $8.76 \pm 0.24 \mu\text{m}$  for tethered cells to  $9.09 \pm 0.27 \mu\text{m}$  for suspension cells (Figure 5b). Statistical differences were not observed between tethered and suspension states.

The fluorescence information from the z-stacks can also be used to estimate the cell volume under all three conditions (see Methods and Figure S5). Here, our data from experimental triplicates showed a significant decrease from  $3,035 \pm 148 \mu\text{m}^3$  for adherent cells ( $n = 66$ ) to  $2,959 \pm 134 \mu\text{m}^3$  and  $2,309 \pm 109 \mu\text{m}^3$  for tethered ( $n = 81$ ) and suspension cells ( $n = 73$ ), respectively (Figure 5c). Importantly, an alternative approach to calculate the volume of  $n = 6,582$  suspended cells from RT-DC reservoir data utilizing their rotational symmetry inside the microfluidic channel yields a very similar result of  $1964 \pm 53 \mu\text{m}^3$  and confirmed our approach. Interestingly, we observe an inverse relationship between volume and Young's modulus across adherent, tethered and suspended cells, where suspended cells have the smallest volume and the largest Young's modulus (Figure 5d).

## 3 | DISCUSSION

Adherent cells actively communicate with their microenvironment, and in the course of physiological events, cells demonstrate dynamics in the focal adhesion complexes (Wolfenson et al., 2009). The intense cytoskeletal changes together with adhesion dynamics result in the loss of interactions with the surface, enabling cells to enter a

suspended state. While this largely depends on the cell type, it is not infrequent and has been reported in a variety of contexts such as cell migration (Trepatt et al., 2012), cell homing, and tissue regeneration (Liesveld et al., 2020), wound healing (ter Horst et al., 2018), and during cancer development (Fares et al., 2020).

In our work, we first focused on the role of seeding density in defining cell elastic and morphological properties. This question is important, given that earlier studies reported a link between cellular crowding and physiological events such as cell spreading, the extent of focal adhesion formation, cytoskeletal tension (Nelson et al., 2004) and cellular differentiation (Hsiao et al., 2016). Within the range used in our study, we observed a significant decrease in cell size with increasing cell density while Young's modulus remained statistically unaltered. Force spectroscopy experiments on a number of cell types using atomic force microscopy demonstrated a cell stiffness vs. seeding density relationship that is either in line (Lee et al., 2021) or in contrast (Efremov et al., 2013; Guo, Bonin, et al., 2014) with our results. Guo and others probed human mammary epithelial cells above the nucleus and reported that cells cultured at higher seeding densities are stiffer than those maintained at lower densities (Guo, Bonin, et al., 2014). However, their measurements consistently made above the nucleus introduce a bias towards changes in nuclear mechanics. It was previously shown that the position at which the cell is probed affects the outcome of Young's modulus determined by AFM (Wu et al., 2018). In particular, when mechanical properties are analyzed in the nuclear region, a higher Young's modulus relative to cytoplasmic regions is typically detected (Mathur et al., 2000; Wu et al., 2018; Yousafzai et al., 2016). In contrast to that study (Guo, Bonin, et al., 2014), when the mammary epithelial cells were indented up to  $1 \mu\text{m}$  in depth to mitigate the nuclear contribution on cellular elasticity, Young's modulus in the range of  $1 \text{ kPa}$  was reported independent of seeding density (Lee et al., 2021). Although being carried out on HEK293T cells, our results are in good agreement with this latter study, which can be explained by the fact that RT-DC probes predominantly cytoplasmic contributions to cell mechanics with limited impact from the nucleus (Urbanska et al., 2020). Taken together our data demonstrates that seeding density impacts cell size in agreement with previous reports (Venugopal et al., 2018) but not on the cytoplasmic contributions to cell elasticity.

In the next step, we compared the mechanical properties of HEK293T cells in adherent, tethered and suspended states. Force spectroscopy measurements on a substrate were carried out using AFM, while cells in suspension were characterized by RT-DC. Comparisons between cell mechanical assays using varying techniques should always be evaluated with care, however, earlier studies have demonstrated that RT-DC and AFM measurements can arrive at similar results despite methodological differences and discrepancies in sample preparation (Pires et al., 2019; Pires et al., 2022). Having established a negligible impact on Young's modulus, we chose to work at seeding densities of approximately  $30,000 \text{ cells}/\text{cm}^2$  corresponding to approximately 50–60% confluence. Our results indicate that Young's modulus of HEK293T cells decreases with increasing levels of cell-surface adherence. Although softening of HEK293T cells under

these conditions has been reported before (Haghparast et al., 2015) it has to be emphasized that this observation is not universal and depends on the cell type being investigated (Haghparast et al., 2013). Interestingly, our study shows a pronounced standard deviation for Young's modulus of tethered cells, which suggest that they possess mechanical features of both adherent and suspended cells.

To gain better insight into the biology associated with our mechanical observations, we looked into morphological and cytoskeletal cell features. Here, we focused on the role of filamentous actin (F-actin), since the interplay between this structural protein, cell mechanics (Golfier et al., 2017; Kita et al., 2021; Kräter et al., 2018; Liu et al., 2020; Pires et al., 2019) as well as cell morphology is well established (Clark & Paluch, 2011; Park et al., 2010). Our results reveal that adherent cells are spread out and present possible focal adhesion points to the surface in accordance with earlier observations (Haghparast et al., 2015). Following detachment, tethered HEK293T cells become globular yet retained some of their surface attachment foci that are dissipated in suspended cells which appear to display a much more globular shape. Thus, within the timescale of our experiments, the presence of a surface seems to have little impact on the average density of F-actin within the cell as well as inside the cell cortex.

With tethered cells displaying mechanical and cytoskeletal features of adherent as well as suspended cells, we looked into the role of cell morphology and its relation to cell stiffening upon loss of surface contacts. In our study, we observed an increase in circularity from adherent to tethered and to suspended cells. This is in agreement with the findings by Tachibana et al., who reported on cell stiffening associated with increased cell circularity, possibly by phosphorylation of Ezrin/Radixin/Moesin (ERM) proteins (Tachibana et al., 2015). Once phosphorylated, these proteins acquire an active conformational state and establish a link between the plasma membrane and F-actin thereby strengthening the cell cortex. This mechanism has also been reported in rounding of cells during mitosis (Fehon et al., 2010) and in tumor cells associated with a reduced invasion capability (Tsujita et al., 2021), where cell rounding correlates with increased cell stiffening. Taken together, these reports strengthen our observation that the configuration of F-actin, but not its levels play a crucial role in determining the cell elasticity.

In addition to alterations in circularity, we observed occasional blebbing of the cells in tethered state, which were undetected in suspended and adherent cells. Blebbing of detached cells has been reported earlier and attributed to its reattachment efforts (Erickson & Trinkaus, 1976; Norman et al., 2010). Studies by Chan et al. (2015), and Maloney et al. (2010), showed the dependency of blebbing on Young's modulus where cell stiffening is correlated with the reduction of the blebs in suspended cells. This is in direct agreement with the stiffening of suspended cells without blebs compared to the cells in tethered state with blebs. It has been reported that bleb retraction is accompanied by the recruitment of Ezrin protein to the plasma membrane thereby stabilizing the actin cortex in the cell (Charras et al., 2006). Conceivably, this could explain the possible role of ERM

proteins in stiffening the suspended cells from tethered cells as the proportion of blebs decreases respectively.

We also looked into the possible effect of cell-surface attachment on cell volume and the correlation between volume and Young's modulus. Changes in cell volume are manifested as a result of alterations in cell physiology (Glykys et al., 2017; Hoffmann et al., 2009; Sun & Kahle, 2014) also associated with changes in cellular elasticity (Danahe et al., 2021; Guo et al., 2017). Our results indicate that tethered and adherent cells have a similar volume while bringing cells into suspension leads to a decrease in volume by 30%. Interestingly, there appears to be a correlation between cell volume and cellular elasticity, wherein suspended cells with lowest volume have the largest Young's modulus. In fact, such an inverse trend has been reported earlier in different cell types (Guo et al., 2017; Sunnerberg et al., 2019; Zhou et al., 2009). Earlier reports suggest that due to the efflux of water from cells, cellular volume decreases along with an increase in the macromolecular density thereby stiffening the cells (Guo et al., 2017). Extrapolating such an inverse correlation between Young's modulus and cellular volume to the current study, it would be expected for adherent and tethered cells to have similar volumes and Young's moduli. While our results confirm the hypothesis of similar volumes, we report an increase in stiffness from adherent to tethered state, which could be linked to cellular circularity and the onset of blebbing. These findings highlight the crucial role of morphological features of cells and their association with cell elasticity. Proteins regulating cell volume as well as the cytoskeleton might be of importance to link these phenomena. Here, transport protein Na-H exporter protein 1 would be a candidate given its contribution in controlling volume (Vallés et al., 2015) and its association with F-actin organization (Denker & Barber, 2002). Further studies on this class of transport proteins might unveil these co-dependencies.

In summary, we investigated the impact of seeding density and cell-surface interactions on the molecular, morphological, and mechanical properties of HEK293T cells. While Young's modulus is independent of seeding density, we observed increased cell stiffening in response to the loss of surface contacts. These changes in mechanical properties are not driven by dynamic alterations in F-actin density but correlate with cell circularity and volume.

## 4 | MATERIALS AND METHODS

### 4.1 | Cell culture

Human embryonic kidney 293 T (HEK293T) cells were cultured and maintained in DMEM high glucose medium (Biowest, Germany) supplemented with 10% FCS (Gibco, Germany) and 2 mM L-glutamine (Biowest, Germany) at 37°C and 5% CO<sub>2</sub>. Cultures were passaged at 70–80% confluency using Trypsin-EDTA (Biowest, Germany) and routinely checked for the presence of mycoplasma contamination by the respective genomic detection by polymerase chain reaction (PCR) (NEB, Germany).



## 4.2 | Sample preparation

Cell seeding experiments were carried out at densities of  $16 \times 10^3$ ,  $40 \times 10^3$ ,  $100 \times 10^3$ , and  $160 \times 10^3$  cells/cm<sup>2</sup> corresponding to a confluence of approximately 30%, 50%, 90%, and 98% respectively. For cell-surface interaction experiments, cells were seeded initially at a density of  $4 \times 10^3$  cells/cm<sup>2</sup> and cultured for 72 h to attain an approximate density of  $30 \times 10^3$  cells/cm<sup>2</sup> with confluency between 50% and 60%. Cultured cells were either probed attached to the surface (adherent state), probed after detachment from the surface (suspended state), or probed after detachment followed by non-specific anchoring to the surface via a linker molecule (tethered state). To prepare cells in suspended and tethered states, cells were first detached by incubation with  $1 \times$  TrypLE (ThermoFisher Scientific, Germany) for 5 min and the procedure was stopped with the addition of DMEM high glucose medium supplemented with 10% FCS. Detached cells were harvested by centrifugation at  $200 \times$  RCF for 5 min and the cell pellet was either resuspended for analysis (suspended state) or further anchored to a polymer-coated surface (tethered state). Tethering of suspended cells to the surface was accomplished using a non-specific biocompatible anchor for cell membrane molecule (BAM / SUNB-RIGHT OE-020CS, NOF Corporation, Japan) consisting of a copolymer of polyethylene glycol (PEG) with oleic acid and further modified with an N-hydroxysuccinimide moiety. BAM-coated surfaces were prepared with modifications according to an earlier report (Haghparast et al., 2013). Briefly, the cell-culture surfaces were coated with 5% BSA (Sigma-Aldrich, Germany) in PBS for 1 h. After washing with PBS, the surface was treated with 1 mM BAM (in PBS) for 30 min at room temperature. Subsequently, the supernatant was aspirated, and the surfaces were further incubated in PBS for 30 min at 37°C, washed again with PBS and left to dry at room temperature for 10 min. Freshly harvested cells were deposited onto BAM-coated surfaces and maintained in DMEM high glucose medium with 10% FCS and 2 mM L-glutamine for 30 min at 37°C and 5% CO<sub>2</sub>. Unanchored cells were removed prior to measurements by an additional washing step.

## 4.3 | Real-time deformability cytometry

Cultures at seeding densities of  $16 \times 10^3$ ,  $40 \times 10^3$ ,  $60 \times 10^3$ ,  $100 \times 10^3$ , and  $160 \times 10^3$  cells/cm<sup>2</sup>, were detached as described above and the cell pellet was resuspended in 100  $\mu$ l of Cell Carrier A buffer (CCA, PBS without Ca<sup>2+</sup> and Mg<sup>2+</sup>, Zellmechanik Dresden, Germany) at a density of approximately  $1 \times 10^6$  cells/ml. Cell size and deformation were measured using an AcCellerator system (Zellmechanik Dresden GmbH, Germany) by flushing the cell suspension through a squared channel of 300  $\mu$ m length and a cross-section of  $30 \times 30 \mu\text{m}^2$ . In all our experiments we used a flow rate of 0.24  $\mu$ l/s. Images of the cells were acquired by a CMOS camera and analyzed in real-time using the software Shapeln (version 2.0.5, Zellmechanik Dresden, Germany) from which cell deformation  $D$  was calculated (Mietke et al., 2015; Otto et al., 2015) by:

$$D = 1 - \frac{2\sqrt{\pi A}}{P}, \quad (1)$$

where  $P$  is the perimeter and  $A$  is the projected area of the cell.

Using an analytical and numerical model (Mietke et al., 2015; Mokbel et al., 2017), Young's modulus of all cells was calculated by the software ShapeOut (version 0.9.0., Zellmechanik Dresden, Germany). During the analysis, a gating range of cell sizes between 50  $\mu\text{m}^2$  and 800  $\mu\text{m}^2$  was applied to eliminate any debris from the events acquired. In addition, an area-ratio filter of 1.05 was employed to exclude incorrectly tracked cells by allowing a deviation of 5% between the convex hull area and the contour area.

## 4.4 | Force spectroscopy

Cell indentation experiments were carried out at room temperature on an atomic force microscope (Nanowizard 3, JPK instruments, Germany) using tipless cantilevers with a nominal spring constant of 0.03 N/m (HQ:CSC38/Al BS, Micromasch, Germany), which were experimentally calibrated by thermal method (Hutter & Bechhoefer, 1998). A single SiO<sub>2</sub> bead was attached to the cantilever by an adhesive film (Norland Products, USA) cured by exposure to 365 nm light for 20 min.

Adherent and tethered cells were probed on glass bottom WillCo-dishes (Willco wells, The Netherlands). For assessing the mechanical properties of tethered samples, freshly detached cells were anchored onto a BAM-coated surface at a density of  $10 \times 10^3$  cells/cm<sup>2</sup>. Samples were indented at an extended speed of 2  $\mu\text{m/s}$  to a depth of typically 1  $\mu\text{m}$  over multiple scanning areas with  $20 \times 20 \mu\text{m}^2$  in size comprising  $5 \times 5$  probing sites.

The Hertz model of a spherical indenter was applied to analyze force-indentation curves following the equation:

$$F = \frac{4ER^{1/2}}{3(1-\nu^2)} \delta^{3/2}, \quad (2)$$

where  $F$  is the indentation force,  $E$  is the cellular elasticity,  $R$  is the radius of the SiO<sub>2</sub> bead ( $2.40 \pm 0.10 \mu\text{m}$ ),  $\nu$  is the Poisson's ratio (here corresponds to 0.5) and  $\delta$  is the depth of indentation. For cells in tethered and adherent states, 100 of measurements were carried out per condition and the study involved three experimental replicates per condition.

## 4.5 | Confocal laser scanning fluorescence microscopy

Fluorescence microscopy was used to evaluate the cytoskeleton between different conditions. Samples of adherent cells were prepared by seeding them in imaging chambers (Ibidi, Germany) at  $25 \times 10^3$  cells/cm<sup>2</sup> followed by a 24 h culture period before imaging. Equally, samples of suspension cells were produced by first seeding

them at  $25 \times 10^3$  cells/cm<sup>2</sup> followed by a 24 h culture period and subsequent proteolytic detachment. Afterwards, cells were fixed, washed, labeled for F-actin and imaged as detailed below. Preparation of samples containing tethered cells involved seeding them at  $50 \times 10^3$  cells/cm<sup>2</sup>, followed by a 24 h culture period. Afterwards, they were proteolytically detached and left to anchor onto the surface of BAM-coated imaging chambers at a density of  $25 \times 10^3$  cells/cm<sup>2</sup> as described above.

Cells in adherent, tethered or suspension states were fixed in a fixing solution consisting of PBS and 4% paraformaldehyde (Sigma-Aldrich, Germany) for 15 min and washed with PBS containing 1% BSA (wash buffer). Washing of suspension cells was performed by centrifugation at  $1000\times$  RCF. Subsequently, cells were permeabilized in PBS with 0.5% Triton X (Sigma-Aldrich, Germany) for 15 min followed by washing, and then incubated for 15 min at room temperature in the presence of a fluorescent label before being washed and subsequently imaged. Labelling of F-actin was achieved using phalloidin conjugated with tetramethylrhodamine (TRITC) (ThermoFisher Scientific, Germany). Suspension cells were immobilized by cytocentrifugation at  $113\times$  RCF for 5 min prior to imaging.

Cells were imaged on a Zeiss confocal laser scanning microscope (LSM 980 with Airyscan 2, Carl Zeiss Inc, Germany) using a  $20\times$  objective with a numerical aperture (NA) of 0.8 corresponding to a pixel size of the optical system of  $0.11 \mu\text{m}/\text{pixel}$ . In addition, imaging was performed using a  $63\times$  oil-immersion objective with  $\text{NA} = 1.4$  corresponding to a pixel size of the optical system of  $0.03 \mu\text{m}/\text{pixel}$ . TRITC was excited by a 561 nm HeNe laser, and the fluorescence was recorded at the respective emission wavelength. To calculate the cell volume, image stacks were acquired over  $20.5 \mu\text{m}$  along the z-axis with the  $20\times$  objective resulting in 41 slices, each with a thickness of  $0.5 \mu\text{m}$ .

#### 4.6 | Image analysis

Analysis of fluorescence intensity of TRITC-conjugated phalloidin in HEK293T cells was performed using proprietary Zeiss imaging and analysis software (Zen v. 3.3.89, Carl Zeiss Inc, Germany). The segmentation workflow involved image binarization using the thresholding range of 10–65,000 pixels, followed by a morphological fill-holes operation to identify particles larger than  $20 \mu\text{m}^2$ . Smaller particles were considered debris and excluded from the analysis. From a single focal plane with highest fluorescent signal, we measured the F-actin density in the cell and cell-cortex as well as cell circularity. The F-actin density was assessed by integrating the fluorescence intensity of the TRITC-phalloidin signal from a single focal plane and dividing it by the respective cell area. To assess the levels of cortical F-actin, a ring-shaped mask of  $1 \mu\text{m}$  width was used to collect the integrated intensity of the fluorescent signal in the cortical region of cells.

For cell height and volume calculations, image stacks of cells labeled for F-actin were first cropped in Fiji/ImageJ (Schindelin et al., 2012) to isolate individual cells and the fluorescence intensity

was integrated on each image plane along the z-axis. The cell height was approximated to the full width at half maximum (FWHM) of the integrated fluorescence intensity profile along the z-axis using the data analysis software package OriginPro (version 9.8.0.200, OriginLab, USA). For cell volume analysis, image segmentation was carried out as described above to yield the area occupied by a cell in each slice of the z-stack. Cell volume  $V$  was estimated by defining it as:

$$V = \sum hA_i, \quad (3)$$

where  $h$  is the thickness of each slice ( $0.5 \mu\text{m}$ ) and  $A$  is the detected area of the cell in each  $i$  slice.

Volume of suspended cells determined by confocal fluorescence imaging data was compared to the volume obtained from brightfield images extracted from RT-DC measurements, which was calculated based on the area defined by the cell contour and assuming rotational symmetry (Herbig et al., 2018).

#### 4.7 | Statistical analysis

All statistical analyses were performed using algorithms written in R language (R Core Team, 2020). These included: (a) the *lme4* package, for the assessment of significance by means of linear mixed models (Bates et al., 2015) where replication was considered as a source of random effects while seeding density and attachment condition were assigned as fixed effects in the respective studies; for the analysis of Young's modulus, culture-day was also considered as a random effect (b) the *emmeans* package, for reporting of estimated marginal means and variances (Searle et al., 1980) (c) as well as the *ggplot2* package, for assembly of violin plots (Wickham, 2009).

#### AUTHOR CONTRIBUTIONS

OO and RHP designed the research. VASD carried out cell culture, sample preparation, RT-DC assays, performed confocal microscopy, image analysis, and statistical analysis. EM performed force spectroscopy measurements. PN generated force-distance curves based on force spectroscopy measurements. DB performed cell culture. VASD wrote the manuscript. OO and RHP reviewed the manuscript.

#### ACKNOWLEDGMENTS

The authors kindly acknowledge financial support from the German Federal Ministry of Education and Research (ZIK grant to OO under grant agreements 03Z22CN11 and 03Z22C511) and the German Center for Cardiovascular Research (Postdoc startup grant 81X3400107 to OO). Open Access funding enabled and organized by Projekt DEAL.

#### CONFLICT OF INTEREST

OO is a shareholder of Zellmechanik Dresden GmbH distributing real-time deformability cytometry. All other authors do not report any conflict of interest.

## DATA AVAILABILITY STATEMENT

The data that support the findings of this study are available from the corresponding author upon reasonable request. The file formats of the raw data are CZI for confocal images, RTDC for RT-DC data.

## ORCID

Venkata A. S. Dabbiru  <https://orcid.org/0000-0002-8140-4335>

Doreen Biedenweg  <https://orcid.org/0000-0002-4175-2618>

Peter Nestler  <https://orcid.org/0000-0003-2275-5706>

Oliver Otto  <https://orcid.org/0000-0003-0280-5374>

## REFERENCES

- Bates, D., Mächler, M., Bolker, B. M., & Walker, S. C. (2015). Fitting linear mixed-effects models using lme4. *Journal of Statistical Software*, 67, 1–48. <https://doi.org/10.18637/jss.v067.i01>
- Buonsanti, M., Cacciola, M., Megali, G., Morabito, F. C., Pellicano, D., Pontari, A., & Versaci, M. (2009). Mechanical aspects in the cells detachment. *IFMBE Proceedings*, 23, 1842–1845. [https://doi.org/10.1007/978-3-540-92841-6\\_457](https://doi.org/10.1007/978-3-540-92841-6_457)
- Cappella, B. (2016). *Mechanical properties of polymers measured through AFM force-distance curves* (1st ed.). Switzerland: Springer Cham. [https://doi.org/10.1007/978-3-319-29459-9\\_1](https://doi.org/10.1007/978-3-319-29459-9_1)
- Chan, C. J., Ekpenyong, A. E., Golfier, S., Li, W., Chalut, K. J., Otto, O., ... Lautenschläger, F. (2015). Article myosin II activity softens cells in suspension. *Biophysj*, 108, 1856–1869. <https://doi.org/10.1016/j.bpj.2015.03.009>
- Charras, G. T., Hu, C. K., Coughlin, M., & Mitchison, T. J. (2006). Reassembly of contractile Actin cortex in cell blebs. *The Journal of Cell Biology*, 175, 477–490. <https://doi.org/10.1083/jcb.200602085>
- Clark, A. G., & Paluch, E. (2011). Mechanics and regulation of cell shape during the cell cycle. *Results and Problems in Cell Differentiation*, 53, 31–73. [https://doi.org/10.1007/978-3-642-19065-0\\_3](https://doi.org/10.1007/978-3-642-19065-0_3)
- Danahe, M., Park, C. Y., Fredberg, J. J., & Weitz, D. A. (2021). Tumorigenic mesenchymal clusters are less sensitive to moderate osmotic stresses due to low amounts of junctional E-cadherin. *Scientific Reports*, 11, 1–12. <https://doi.org/10.1038/s41598-021-95740-x>
- Denker, S. P., & Barber, D. L. (2002). Ion transport proteins anchor and regulate the cytoskeleton. *Current Opinion in Cell Biology*, 14, 214–220. [https://doi.org/10.1016/S0955-0674\(02\)00304-6](https://doi.org/10.1016/S0955-0674(02)00304-6)
- Denning, C., Borgdorff, V., Crutchley, J., Firth, K. S. A., George, V., Kalra, S., ... Young, L. E. (2016). Cardiomyocytes from human pluripotent stem cells: From laboratory curiosity to industrial biomedical platform. *Biochimica et Biophysica Acta*, 1863, 1728–1748. <https://doi.org/10.1016/j.bbamcr.2015.10.014>
- Efremov, Y. M., Dokrunova, A. A., Bagrov, D. V., Kudryashova, K. S., Sokolova, O. S., & Shaitan, K. V. (2013). The effects of confluency on cell mechanical properties. *Journal of Biomechanics*, 46, 1081–1087. <https://doi.org/10.1016/j.jbiomech.2013.01.022>
- Ekpenyong, A. E., Toepfner, N., Chilvers, E. R., & Guck, J. (2015). Mechano-transduction in neutrophil activation and deactivation. *Biochimica et Biophysica Acta*, 1853, 3105–3116. <https://doi.org/10.1016/j.bbamcr.2015.07.015>
- Erickson, C. A., & Trinkaus, J. P. (1976). Microvilli and blebs as sources of reserve surface membrane during cell spreading. *Experimental Cell Research*, 99, 375–384. [https://doi.org/10.1016/0014-4827\(76\)90595-4](https://doi.org/10.1016/0014-4827(76)90595-4)
- Fares, J., Fares, M. Y., Khachfe, H. H., Salhab, H. A., & Fares, Y. (2020). Molecular principles of metastasis: A hallmark of cancer revisited. *Signal Transduction and Targeted Therapy*, 5, 1–17. <https://doi.org/10.1038/s41392-020-0134-x>
- Fehon, R. G., McClatchey, A. I., & Bretscher, A. (2010). Organizing the cell cortex: The role of ERM proteins. *Nature Reviews Molecular Cell Biology*, 11, 276–287. <https://doi.org/10.1038/nrm2866>
- Fife, C. M., McCarroll, J. A., & Kavallaris, M. (2014). Movers and shakers: Cell cytoskeleton in cancer metastasis. *British Journal of Pharmacology*, 171, 5507–5523. <https://doi.org/10.1111/bph.12704>
- Fletcher, D. A., & Mullins, R. D. (2010). Cell mechanics and the cytoskeleton. *Nature*, 463, 485–492. <https://doi.org/10.1038/nature08908>
- Glykys, J., Dzhalal, V., Egawa, K., Kahle, K. T., Delpire, E., & Staley, K. (2017). Chloride dysregulation, seizures, and cerebral edema: A relationship with therapeutic potential. *Trends in Neurosciences*, 40, 276–294. <https://doi.org/10.1016/j.tins.2017.03.006>
- Golfier, S., Rosendahl, P., Mietke, A., Herbig, M., Guck, J., & Otto, O. (2017). High-throughput cell mechanical phenotyping for label-free titration assays of cytoskeletal modifications. *Cytoskeleton*, 74, 283–296. <https://doi.org/10.1002/cm.21369>
- Guo, J., Wang, Y., Sachs, F., & Meng, F. (2014). Actin stress in cell reprogramming. *Proceedings of the National Academy of Sciences of the United States of America*, 111, E5252–E5261. <https://doi.org/10.1073/PNAS.1411683111>
- Guo, M., Pegoraro, A. F., Mao, A., Zhou, E. H., Arany, P. R., Han, Y., ... Weitz, D. A. (2017). Cell volume change through water efflux impacts cell stiffness and stem cell fate. *Proceedings of the National Academy of Sciences of the United States of America*, 114, E8618–E8627. <https://doi.org/10.1073/PNAS.1705179114>
- Guo, X., Bonin, K., Scarpinato, K., Guthold, M., Guo, X., Bonin, K., ... Guthold, M. (2014). The effect of neighboring cells on the stiffness of cancerous and non-cancerous human mammary epithelial cells. *NJPh*, 16, 105002. <https://doi.org/10.1088/1367-2630/16/10/105002>
- Haase, K., & Pelling, A. E. (2015). Investigating cell mechanics with atomic force microscopy. *Journal of the Royal Society Interface*, 12, 20140970. <https://doi.org/10.1098/rsif.2014.0970>
- Haghighparast, S. M. A., Kihara, T., & Miyake, J. (2015). Distinct mechanical behavior of HEK293 cells in adherent and suspended states. *PeerJ*, 3, e1131. <https://doi.org/10.7717/peerj.1131>
- Haghighparast, S. M. A., Kihara, T., Shimizu, Y., Yuba, S., & Miyake, J. (2013). Actin-based biomechanical features of suspended normal and cancer cells. *Journal of Bioscience and Bioengineering*, 116, 380–385. <https://doi.org/10.1016/j.jbiosc.2013.03.003>
- Herbig, M., Kräter, M., Plak, K., Müller, P., Guck, J., & Otto, O. (2018). Real-time deformability cytometry: Label-free functional characterization of cells. *Methods in Molecular Biology*, 1678, 347–369. [https://doi.org/10.1007/978-1-4939-7346-0\\_15](https://doi.org/10.1007/978-1-4939-7346-0_15)
- Hoffmann, E. K., Lambert, I. H., & Pedersen, S. F. (2009). Physiology of cell volume regulation in vertebrates. *Physiological Reviews*, 89, 193–277. <https://doi.org/10.1152/physrev.00037.2007>
- Hsiao, C., Lampe, M., Nillasithanukroh, S., Han, W., Lian, X., & Palecek, S. P. (2016). Human pluripotent stem cell culture density modulates YAP signaling. *Biotechnology Journal*, 11, 662–675. <https://doi.org/10.1002/biot.201500374>
- Hutter, J. L., & Bechhoefer, J. (1998). Calibration of atomic-force microscope tips. *Review of Scientific Instruments*, 69, 1868–1873. <https://doi.org/10.1063/1.1143970>
- Kihara, T., Haghighparast, S. M. A., Shimizu, Y., Yuba, S., & Miyake, J. (2011). Physical properties of mesenchymal stem cells are coordinated by the perinuclear Actin cap. *Biochemical and Biophysical Research Communications*, 409, 1–6. <https://doi.org/10.1016/j.bbrc.2011.04.022>
- Kita, K., Asanuma, K., Okamoto, T., Kawamoto, E., Nakamura, K., Hagi, T., ... Sudo, A. (2021). Cytoskeletal Actin structure in osteosarcoma cells determines metastatic phenotype via regulating cell stiffness, migration, and transmigration. *Current Issues in Molecular Biology*, 43, 1255–1266. <https://doi.org/10.3390/cimb43030089>
- Kräter, M., Sapudom, J., Bilz, N. C., Pompe, T., Guck, J., & Claus, C. (2018). Alterations in cell mechanics by Actin cytoskeletal changes correlate with strain-specific rubella virus phenotypes for cell migration and induction of apoptosis. *Cell*, 7, 136. <https://doi.org/10.3390/cells7090136>

- Lautenschläger, F., Paschke, S., Schinkinger, S., Bruel, A., Beil, M., & Guck, J. (2009). The regulatory role of cell mechanics for migration of differentiating myeloid cells. *Proceedings of the National Academy of Sciences of the United States of America*, 106, 15696–15701. <https://doi.org/10.1073/pnas.0811261106>
- Lee, H., Bonin, K., & Guthold, M. (2021). Human mammary epithelial cells in a mature, stratified epithelial layer flatten and stiffen compared to single and confluent cells. *Biochimica et Biophysica Acta (BBA) - General Subjects*, 1865, 129891. <https://doi.org/10.1016/j.bbagen.2021.129891>
- Lekka, M., & Pabijan, J. (2019). Measuring elastic properties of single cancer cells by AFM. *Methods in Molecular Biology*, 1886, 315–324. [https://doi.org/10.1007/978-1-4939-8894-5\\_18](https://doi.org/10.1007/978-1-4939-8894-5_18)
- Liesveld, J. L., Sharma, N., & Aljitiawi, O. S. (2020). Stem cell homing: From physiology to therapeutics. *Stem Cells*, 38, 1241–1253. <https://doi.org/10.1002/stem.3242>
- Liu, Y., Mollaeian, K., Shamim, M. H., & Ren, J. (2020). Effect of F-Actin and microtubules on cellular mechanical behavior studied using atomic force microscope and an image recognition-based cytoskeleton quantification approach. *International Journal of Molecular Sciences*, 21, 392. <https://doi.org/10.3390/ijms21020392>
- Maloney, J. M., Nikova, D., Lautenschläger, F., Clarke, E., Langer, R., Guck, J., & van Vliet, K. J. (2010). Mesenchymal stem cell mechanics from the attached to the suspended state. *Biophysical Journal*, 99, 2479–2487. <https://doi.org/10.1016/j.bpj.2010.08.052>
- Mathur, A. B., Truskey, G. A., & Reichert, W. M. (2000). Atomic force and Total internal reflection fluorescence microscopy for the study of force transmission in endothelial cells. *Biophysical Journal*, 78, 1725–1735. [https://doi.org/10.1016/S0006-3495\(00\)76724-5](https://doi.org/10.1016/S0006-3495(00)76724-5)
- Mietke, A., Otto, O., Girardo, S., Rosendahl, P., Taubenberger, A., Golfier, S., ... Fischer-Friedrich, E. (2015). Extracting cell stiffness from real-time deformability cytometry: Theory and experiment. *Biophysical Journal*, 109, 2023–2026. <https://doi.org/10.1016/j.bpj.2015.09.006>
- Mokbel, M., Mokbel, D., Mietke, A., Träber, N., Girardo, S., Otto, O., ... Aland, S. (2017). Numerical simulation of real-time deformability cytometry to extract cell mechanical properties. *ACS Biomaterials Science and Engineering*, 3, 2962–2973. <https://doi.org/10.1021/acsbomaterials.6b00558>
- Nelson, C. M., Pirone, D. M., Tan, J. L., & Chen, C. S. (2004). Vascular endothelial-cadherin regulates cytoskeletal tension, cell spreading, and focal adhesions by stimulating RhoA. *Molecular Biology of the Cell*, 15, 2943–2953. <https://doi.org/10.1091/mbc.e03-10-0745m>
- Norman, L. L., Bruges, J., Sengupta, K., Sens, P., & Aranda-Espinoza, H. (2010). Cell Blebbing and membrane area homeostasis in spreading and retracting cells. *Biophysical Journal*, 99, 1726–1733. <https://doi.org/10.1016/j.bpj.2010.07.031>
- Otto, O., Rosendahl, P., Mietke, A., Golfier, S., Herold, C., Klau, D., ... Guck, J. (2015). Real-time deformability cytometry: On-the-fly cell mechanical phenotyping. *Nature Methods*, 12, 199–202. <https://doi.org/10.1038/nmeth.3281>
- Park, Y. K., Best, C. A., Badizadegan, K., Dasari, R. R., Feld, M. S., Kuriabova, T., ... Popescu, G. (2010). Measurement of red blood cell mechanics during morphological changes. *Proceedings of the National Academy of Sciences*, 107, 6731–6736. <https://doi.org/10.1073/PNAS.0909533107>
- Pires, R. H., Dau, T. H., Manu, E., Shree, N., & Otto, O. (2022). Switching in the expression pattern of Actin isoforms marks the onset of contractility and distinct mechanodynamic behavior during cardiomyocyte differentiation. *Physiological Reports*, 10, e15171. <https://doi.org/10.14814/phy2.15171>
- Pires, R. H., Shree, N., Manu, E., Guzniczak, E., & Otto, O. (2019). Cardiomyocyte mechanodynamics under conditions of Actin remodelling. *Philosophical Transactions of the Royal Society B*, 374, 1471–2970. <https://doi.org/10.1098/rstb.2019.0081>
- R Core Team. (2020). *R: A language and environment for statistical computing*. Vienna, Austria: R Foundation for Statistical Computing. <https://www.R-project.org/>
- Sauer, F., Fritsch, A., Grosser, S., Pawlizak, S., Kießling, T., Reiss-Zimmermann, M., ... Sack, I. (2021). Whole tissue and single cell mechanics are correlated in human brain tumors. *Soft Matter*, 17, 10744–10752. <https://doi.org/10.1039/d1sm01291f>
- Schindelin, J., Arganda-Carreras, I., Frise, E., Kaynig, V., Longair, M., Pietzsch, T., ... Cardona, A. (2012). Fiji: An open-source platform for biological-image analysis. *Nature Methods*, 9, 676–682. <https://doi.org/10.1038/nmeth.2019>
- Searle, S. R., Speed, F. M., & Milliken, G. A. (1980). Population marginal means in the linear model: An alternative to least squares means. *American Statistician*, 34, 216–221. <https://doi.org/10.1080/00031305.1980.10483031>
- Steward, A. J., & Kelly, D. J. (2015). Mechanical regulation of mesenchymal stem cell differentiation. *Journal of Anatomy*, 227, 717–731. <https://doi.org/10.1111/joa.12243>
- Stricker, J., Falzone, T., & Gardel, M. L. (2010). Mechanics of the F-Actin cytoskeleton. *Journal of Biomechanics*, 43, 9–14. <https://doi.org/10.1016/j.jbiomech.2009.09.003>
- Sun, D., & Kahle, K. T. (2014). Dysregulation of diverse ion transport pathways controlling cell volume homeostasis contribute to neuroglial cell injury following ischemic stroke. *Translational Stroke Research*, 5, 1–2. <https://doi.org/10.1007/s12975-014-0324-3>
- Sunnerberg, J. P., Moore, P., Spedden, E., Kaplan, D. L., & Staii, C. (2019). Variations of elastic modulus and cell volume with temperature for cortical neurons. *Langmuir*, 35, 10965–10976. <https://doi.org/10.1021/acs.langmuir.9b01651>
- Tachibana, K., Haghighparast, S. M. A., & Miyake, J. (2015). Inhibition of cell adhesion by phosphorylated Ezrin/radixin/Moesin. *Cell Adhesion and Migration*, 9, 502–512. <https://doi.org/10.1080/19336918.2015.1113366>
- ter Horst, B., Chouhan, G., Moiemmen, N. S., & Grover, L. M. (2018). Advances in keratinocyte delivery in burn wound care. *Advanced Drug Delivery Reviews*, 123, 18–32. <https://doi.org/10.1016/j.addr.2017.06.012>
- Trepatt, X., Chen, Z., & Jacobson, K. (2012). Cell Migration. *Comprehensive Physiology*, 2, 2369–2392. <https://doi.org/10.1002/cphy.c110012>
- Tsujita, K., Satow, R., Asada, S., Nakamura, Y., Arnes, L., Sako, K., ... Itoh, T. (2021). Homeostatic membrane tension constrains cancer cell dissemination by counteracting BAR protein assembly. *Nature Communications*, 12, 1–14. <https://doi.org/10.1038/s41467-021-26156-4>
- Urbanska, M., Muñoz, H. E., Shaw Bagnall, J., Otto, O., Manalis, S. R., di Carlo, D., & Guck, J. (2020). A comparison of microfluidic methods for high-throughput cell deformability measurements. *Nature Methods*, 17, 587–593. <https://doi.org/10.1038/s41592-020-0818-8>
- Vallés, P. G., Bocanegra, V., Gil Lorenzo, A., & Costantino, V. V. (2015). Physiological functions and regulation of the Na<sup>+</sup>/H<sup>+</sup> exchanger [NHE1] in renal tubule epithelial cells. *Kidney and Blood Pressure Research*, 40, 452–466. <https://doi.org/10.1159/000368521>
- Venugopal, B., Mogha, P., Dhawan, J., & Majumder, A. (2018). Cell density overrides the effect of substrate stiffness on human mesenchymal stem cells' morphology and proliferation. *Biomaterials Science*, 6, 1109–1119. <https://doi.org/10.1039/C7BM00853H>
- Wickham, H. (2009). *ggplot2: Elegant graphics for data analysis* (1st ed.). New York, NY: Springer. <https://doi.org/10.1007/978-0-387-98141-3>
- Wolfenson, H., Henis, Y. I., Geiger, B., & Bershadsky, A. D. (2009). The heel and toe of the cell's foot: A multifaceted approach for understanding the structure and dynamics of focal adhesions. *Cell Motility and the Cytoskeleton*, 66, 1017–1029. <https://doi.org/10.1002/cm.20410>
- Wu, P. H., Aroush, D. R. B., Asnacios, A., Chen, W. C., Dokukin, M. E., Doss, B. L., ... Wirtz, D. (2018). A comparison of methods to assess cell

- mechanical properties. *Nature Methods*, 15, 491–498. <https://doi.org/10.1038/s41592-018-0015-1>
- Yousafzai, M. S., Coceano, G., Mariutti, A., Ndoye, F., Ladan, A., Niemela, J., ... Cojoc, D. (2016). Effect of neighboring cells on cell stiffness measured by optical tweezers indentation. *Journal of Biomedical Optics*, 21, 57004. <https://doi.org/10.1117/1.jbo.21.5.057004>
- Zhou, E. H., Trepap, X., Park, C. Y., Lenormand, G., Oliver, M. N., Mijailovich, S. M., ... Fredberg, J. J. (2009). Universal behavior of the osmotically compressed cell and its analogy to the colloidal glass transition. *Proceedings of the National Academy of Sciences of the United States of America*, 106, 10632–10637. <https://doi.org/10.1073/pnas.0901462106>

## SUPPORTING INFORMATION

Additional supporting information can be found online in the Supporting Information section at the end of this article.

**How to cite this article:** Dabbiru, V. A. S., Manu, E., Biedenweg, D., Nestler, P., Pires, R. H., & Otto, O. (2023). Cell-surface contacts determine volume and mechanical properties of human embryonic kidney 293 T cells. *Cytoskeleton*, 80(1-2), 21–33. <https://doi.org/10.1002/cm.21735>